BLADE-VORTEX INTERACTION NOISE OF AN ISOLATED FULL-SCALE XV-15 TILT-ROTOR

C. Kitaplioglu*, M. Betzina*, and W. Johnson*
Army/NASA Rotorcraft Division
NASA Ames Research Center
Moffett Field, California 94035

ABSTRACT

Blade-vortex interaction noise of an isolated full-scale XV-15 tilt-rotor was investigated in the NASA Ames 80- by 120-Foot Wind Tunnel. The objective was to establish the baseline BVI noise signature of a full-scale tilt-rotor and to investigate several noise reduction concepts, including blade-tip subwings, reduced tip Mach number, and the addition of a fourth blade to the rotor system. At the nominal tip Mach number of 0.691, the peak BVI levels were found to occur at a tip-path-plane angle of 4° and at the highest advance ratio tested of 0.2. The BVI noise levels were found to be weakly dependent on C_T/σ. As would be expected, reducing tip Mach number, either of the baseline 3-blade rotor, or in conjunction with a 4-blade rotor, was found to be an effective way to significantly reduce noise. The addition of the tested subwings did not seem to be an effective strategy for noise reduction, and they incurred a performance penalty.

INTRODUCTION

In support of NASA's Short Haul Civil Tiltrotor (SHCT) program, a second phase of a full-scale XV-15 rotor test (Refs. 1 and 2) was performed in the NASA Ames 80- by 120-Foot Wind Tunnel. The present test expanded the operating envelope of the previous test. The overall objective of the test was to establish the baseline blade-vortex interaction (BVI) noise signature of a full-scale tilt-rotor. Additionally, several BVI noise reduction concepts were investigated. These included reduced tip Mach number, blade-tip subwings, and the addition of a fourth blade to the rotor system. This paper presents acoustic results from the wind tunnel test. Some limited data are also included on the influence of the subwings on rotor performance, including comparison with CAMRAD II calculations.

WIND TUNNEL TEST

A full-scale, isolated, right-hand XV-15 rotor was tested in the NASA Ames 80- by 120-Foot Wind Tunnel using the Ames Rotor Test Apparatus (RTA). Figure 1 shows the RTA with the XV-15 rotor installed.

For acoustic measurements, a series of microphones was placed around the model (Fig. 2). Eight microphones traversed a horizontal plane on the advancing side of the rotor 1.8 rotor radii below and 0.2 to 2.0 rotor radii upstream of the rotor hub to measure the BVI noise footprint below the advancing side of the rotor. One fixed microphone (Mic #9) was placed at a position estimated to be along the peak BVI noise radiation direction (at a rotor azimuth of 150° and 20° below the rotor plane; at a distance of 3 rotor diameters from the rotor hub). The wind tunnel test section has a sound absorbing liner which eliminates reflections down to approximately 250 Hz (absorption > 90%). In addition to the liner, sound absorbing foam was attached to portions of the model fuselage to eliminate reflections from its large surface. Additional foam treatment was added to selected points in the test section to eliminate reflection from local hard points.

The testing procedure was to set the tip Mach number (M_{tip}) and advance ratio (μ), then to vary shaft angle (α_s) while maintaining a fixed thrust coefficient / solidity (C_T/σ) and minimizing flapping. The tip-path-plane angle (α_{tpp}) is the sum of α_s and longitudinal flapping, the latter usually being a small value. The initial runs established α_{tpp} for peak BVI noise at each advance ratio tested. Subsequently, detailed acoustic data, including surveys of the acoustic field below the advancing side of the rotor using the traversing microphones, were obtained at various values of

* Aerospace Engineer, Aeromechanics Branch

Presented at the American Helicopter Society 56th Annual Forum, Virginia Beach, Virginia, May 2 – 4, 2000.

advance ratio, tip-path-plane angle, and thrust coefficient at and near this peak BVI condition.

Relevant test parameters, rotor performance data, and acoustic data were recorded and processed on a multi-channel, high-speed data system. The data were digitized at 2048 samples/rev (approximately 20,000 samples/sec) and the acoustic data were anti-alias filtered at 4 kHz. Sixty-four revolutions of data were synchronously averaged per data point. Further processing of the data (power spectra, filtering, etc.) proceeded from this averaged time history. BVI sound pressure levels (BVISPL) were determined by bandpass filtering the data from the 10^{th} to the 50^{th} blade passage harmonic.

Additional details of the wind tunnel test, instrumentation, and data processing can be found in Refs. 1 and 2.

3-BLADE BASELINE ROTOR BVI NOISE

Data for the 3-blade baseline rotor were obtained over a wide range of operating conditions up to advance ratios of 0.2, as shown in Table 1. For most operating conditions, the forward microphone and the traverse microphones showed similar trends. In the following discussion, where appropriate the forward microphone was selected as representative of all the microphones. Bandpass filtered acoustic levels for the forward microphone (Mic #9) at $M_{tip} = 0.691$ and $C_T/\sigma = 0.075$ are shown in Fig. 3 as function of μ and α_{tpp}. No smoothing has been applied to these data and the figure exhibits some kinks due to variations in data which have been extracted from different runs throughout the test. The peak BVISPL levels occur near $\mu = 0.2$ and $\alpha_{tpp} = 4°$. Figure 4 shows BVISPL as function of α_{tpp} at an advance ratio of 0.2 for all the microphones. The traverse was at one rotor radius forward of the hub. This was the location of the highest BVI levels in the majority of cases. For Microphone #9, Fig. 4 is essentially a vertical cut through Fig. 3 at $\mu = 0.2$. The BVI noise levels peak near 4°. A similar horizontal cut at a tip-path-plane angle of 4° shows the variation of BVISPL as function of μ in Fig. 5. The highest BVI levels were measured at the highest tested μ of 0.2. This figure also shows that the traverse microphone (i.e. the lateral location) where the peak BVI level was measured varies with μ. Figure 6a shows BVISPL as function of C_T/σ and indicates that noise levels are quite insensitive to thrust at the highest BVI condition. However, Fig. 6b shows that at a somewhat lower BVI level, there is a relatively weak dependence on C_T/σ.

The unfiltered and bandpass filtered acoustic time histories at the peak BVI condition for the forward microphone (Mic #9) are shown in Figs. 7 and 8. Figure 8(b) shows the details of the middle pulse. The basic characteristic of BVI sound is the high-amplitude pulse. The exact shape, amplitude, and nature of the "tails" on either side of the main pulse depend on the exact operating conditions.

The acoustic footprint under the advancing side of the rotor is shown in Fig. 9 for the peak BVI conditions ($\mu = 0.2$ and $\alpha_{tpp} = 4°$). Two other acoustic footprints at a moderate BVI condition and a low BVI condition are included in Figs 10 and 11. Note that the peak BVI region moves forward as μ decreases and inward as the rotor tip-path-plane rotates down. Figure 12 is the bandpass filtered time history at the low BVI condition. Note the lower amplitude, as well as the change in the pulse shape compared to Fig. 8(b).

BVI NOISE REDUCTION CONCEPTS

Several BVI noise reduction concepts were investigated during the wind tunnel test. These were (1) reduced M_{tip}; (2) installation of small subwings of several different designs at the blade tips; (3) the addition of a fourth identical blade to the rotor system; and (4) use of prescribed and active feedback higher harmonic control. The results of HHC testing, which were quite encouraging, are presented in Ref. 3.

Reduced M_{tip}

Tip Mach number is the single most important determinant of rotor noise. Therefore, an effective way to reduce noise is to reduce rotor RPM. This was investigated during the wind tunnel test in several ways; one being to reduce RPM while maintaining thrust and speed. Reducing RPM while maintaining C_T/σ and μ was also investigated. Figure 13 shows that up to 4 dB noise reduction is possible (at the forward microphone) at the maximum BVI condition with a 10% reduction in M_{tip} (0.691 vs 0.622). The noise footprint at the reduced M_{tip} is shown in Fig. 14. Comparing this to Fig. 10 (at the same thrust and speed, but standard $M_{tip} = 0.691$) shows the significant reduction in the size of the high noise region, and its shift downstream.

Subwings

Trailing tip vortex strength and core size are important parameters for BVI noise. Use of subwings to diffuse the core has been proposed by others as a means for

reducing noise (e.g. Refs. 4 and 5). Two sets of subwings were installed on the baseline 3-bladed rotor to test this idea. Both sets were rectangular in shape and set at fixed incidence angles of +2° or –2° relative to the blade tip. Relative to the chord at the blade tip, they were 0.2 in chord, 0.39 in length, and set back 0.11 from the leading edge. All operating parameters were based on baseline values of blade radius and solidity, no adjustments being made to account for the addition of the subwings.

Figure 15 is a comparison of BVI noise levels of the two subwings with the baseline rotor measured at the forward microphone (Mic #9) at fixed C_T/σ, M_{tip}, and μ over a range of α_{tpp}. Figures 16 – 18 are the acoustic footprints at the same operating conditions near the peak BVI condition, $\alpha_{tpp} = 3°$. The effect of the addition of both sets of subwings was to increase, rather than decrease, the noise.

The influence of the subwings on rotor performance was also examined, including comparison with CAMRAD II calculations. Figure 19 shows measured and calculated power for the XV-15 rotor with and without subwings, as a function of thrust, $\mu = 0.17$, $M_{tip} = 0.691$, and $\alpha_{tpp} = -10°$ (nose down). The measured performance data show a general increase of power required with the subwings installed. There is some effect of subwing angle in the data. The rectangular subwing at –2° gives the smallest increase in power compared to the baseline; the rectangular subwing at +2° produces the largest power increase.

The performance was calculated with CAMRAD II (Ref. 6), using aerodynamic model parameters established through correlation with other tilt-rotor performance and airloads data. Key features of the aerodynamic analysis are the dual-peak wake rollup model (producing negative tip vortex strength when the blade tip has negative loading), and an inboard stall delay model. Both of these features influence the calculated power as a function of thrust. With subwings, the analysis has a rolled up trailed vortex both from the primary blade tip, and from the subwing tip. The calculations were performed with the gimbal motion (trimmed to zero mean gimbal tilt relative the shaft), but without any elastic motion of the blades.

In the calculated performance, the profile and induced power are both increased by the subwing. The propulsive force is reduced with the subwing, and hence the parasite power is reduced. The profile and parasite power changes are about the same magnitude (hence cancel in the change of total power), and about one-third the induced power change. The calculated net power increase is smallest for the +2° subwing and largest for the –2° subwing. The induced power increase produced by the +2° subwing is $\Delta Cp/\sigma = .00019$, that for the –2° subwing $\Delta Cp/\sigma = .00026$. This larger value of induced power is caused by more extensive negative loading at the blade tip for the –2° subwing, compared to the +2° subwing. While the calculated influence of subwing angle is not very great for power, it is more noticeable for the blade loading and wake geometry.

Overall, the correlation between measured and calculated power is good. For the –2° subwing, the measurements and calculation exhibit different trends compared to the other subwing. Work underway on correlation with the baseline XV-15 results may improve the calculated influence of thrust, but probably will not change the calculated influence of the subwing. Little influence has been found of rolled up vortex core size on the calculated performance, with or without the subwing. There might be some influence of blade elasticity for the XV-15. Aerodynamic model deficiencies relevant to these results are calculation of loading on low aspect ratio subwings, and the lack of a representation of merging of the primary and subwing vortices.

4-Blade Rotor

An old idea for reducing rotor noise while maintaining performance is to add an additional rotor blade. The choice is to operate the rotor at the same tip Mach number as the baseline rotor or to reduce the tip Mach number, both while maintaining thrust and speed. Both these ideas were tried during the wind tunnel test. A fourth standard XV-15 blade was added to the rotor using a new hub. This increased the solidity of the rotor. Therefore, for valid comparisons, the 3 - and 4 – blade rotors were operated at fixed thrust (5500 lbs) and airspeed (77 knots), rather than fixed C_T/σ and μ.

Figure 20 is a comparison of the BVI noise, at the forward microphone, of the 3 - and 4 - blade rotors, operated at the same thrust and speed, at both the same and lower M_{tip}. Figures 21 and 22 are the respective acoustic footprints of the 4 - blade rotor at $\alpha_{tpp} = 3°$. The corresponding 3-blade data at $M_{tip} = 0.691$ is shown in Fig. 16. It is clear that noise reductions of as much as 10 dB are possible, but only in conjunction with lower RPM operation.

CONCLUSIONS

An isolated full-scale XV-15 rotor was tested in the NASA Ames 80- by 120-Foot Wind Tunnel. The baseline BVI noise levels over a range of operating conditions were established. At the nominal tip Mach number of 0.691, the peak BVI levels were found to occur at a tip-path-plane angle of 4° and at the highest advance ratio tested of 0.2. The BVI noise levels were found to be weakly dependent on C_T/σ. Several noise reduction ideas were tested and evaluated. As would be expected, reducing tip Mach number, either of the baseline 3-blade rotor, or in conjunction with a 4-blade rotor, is an effective way to significantly reduce noise. Reducing RPM seemed to be about as effective as adding an additional blade without an RPM reduction. However, adding a fourth blade and reducing RPM resulted in a 10 dB BVI noise reduction. The addition of the tested subwings did not seem to be an effective strategy for noise reduction, and they incurred a performance penalty.

ACKNOWLEDGEMENTS

The authors express their appreciation to the test team, led by Robert Fong, for their dedication and support during the performance of the test.

REFERENCES

1. Kitaplioglu, C., McCluer, M., and Acree, Jr., C.W., "Comparison of XV-15 Full-Scale Wind Tunnel and In-Flight Blade-Vortex Interaction Noise," American Helicopter Society 53rd Annual Forum, April, 1997, Virginia Beach, VA.

2. Light, J.S. and Kitaplioglu, C., "Results of the XV-15 Test in the National Full-Scale Aerodynamics Complex", American Helicopter Society 53rd Annual Forum, April, 1997, Virginia Beach, VA.

3. Nguyen, K., Betzina, M., and Kitaplioglu, C., "Full-Scale Demonstration of Higher Harmonic Control for Noise and Vibration Reduction on the XV-15 Rotor," American Helicopter Society 56th Annual Forum, May 2000, Virginia Beach, VA.

4. Tangler, J.L., "Experimental Investigation of the Subwing Tip and Its Vortex Structure," NASA CR-3058, 1978.

5. Lau, B.H., Wadcock, A.J., and Heineck, J.T., "Wake Visualization of a Full-Scale Tilt Rotor in Hover," American Helicopter Society Technical Specialists' Meeting for Rotorcraft Acoustics and Aerodynamics, October, 1997, Williamsburg, Virginia.

6. Johnson, W. "Rotorcraft Aerodynamics Models for a Comprehensive Analysis," American Helicopter Society 54th Annual Forum, May 1998, Washington, DC.

Table 1. Range of Nominal Test Conditions

Parameter	Value
M_{tip}	0.622, 0.691, 0.725
α_s	-15° to +15
μ	0.125, 0.15, 0.17, 0.2
C_T/σ	0.060, 0.075, 0.090, 0.100, 0.120

Fig 1. XV-15 right-hand rotor mounted on the RTA in the NASA Ames 80- by 120-Foot Wind Tunnel.

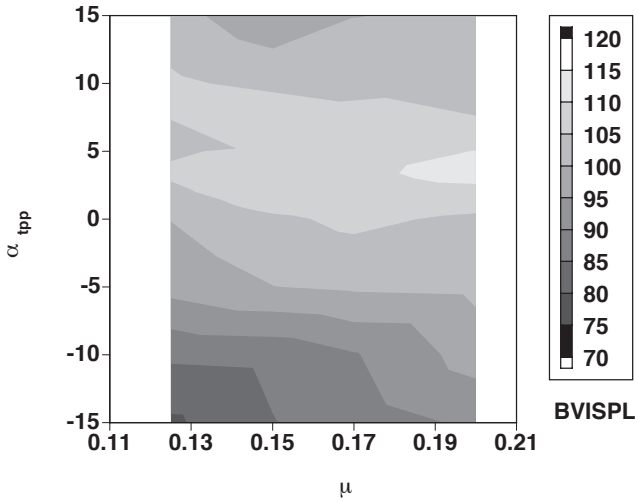

Fig 3. BVISPL as function of μ and α_{tpp}. 3-blade rotor. M_{tip} = 0.691, C_T/σ = 0.075. Mic #9.

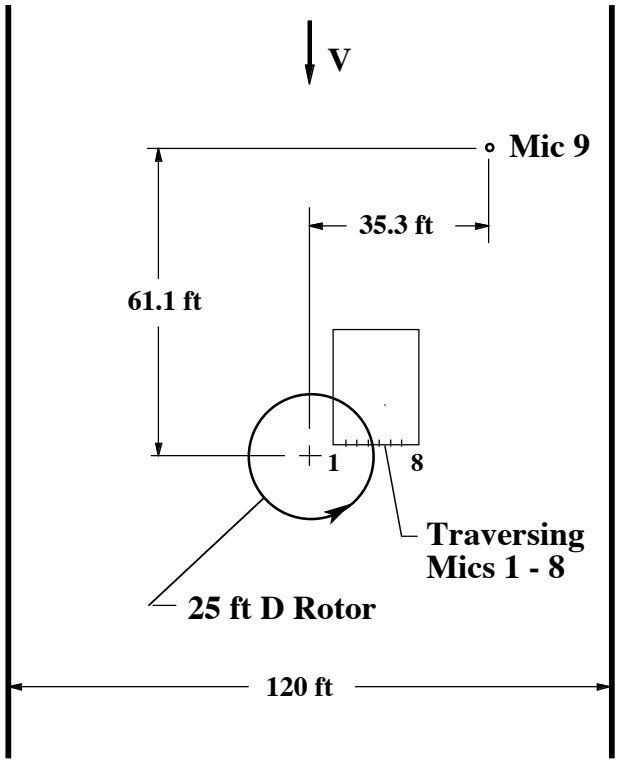

Fig 2. Microphone positions for the XV-15 test in the NASA Ames 80- by 120-Foot Wind Tunnel

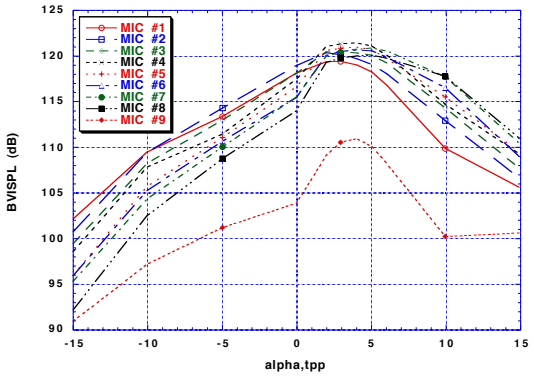

Fig 4. BVISPL as function of α_{tpp} at μ = 0.2. 3-blade rotor. M_{tip} = 0.691, C_T/σ = 0.075. Traverse at r/R = 1.0.

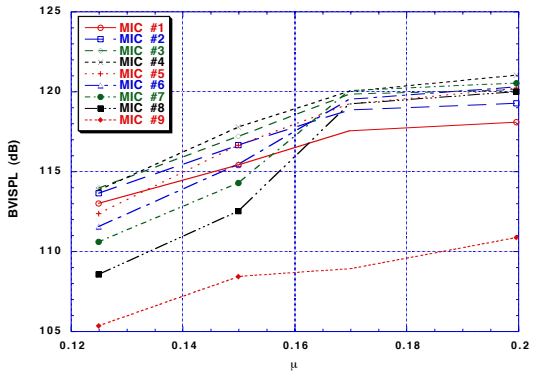

Fig 5. BVISPL as function of μ at α_{tpp} = 4°. 3-blade rotor. M_{tip} = 0.691, C_T/σ = 0.075. Traverse at r/R = 1.0.

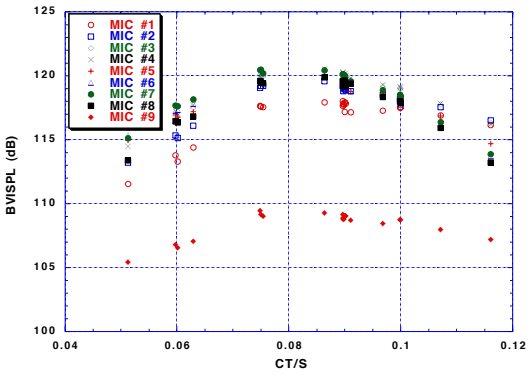

Fig 6b. BVISPL as function of C_T/σ at μ = 0.17 and α_{tpp} = 3°. 3-blade rotor. M_{tip} = 0.691. Traverse at r/R = 1.0.

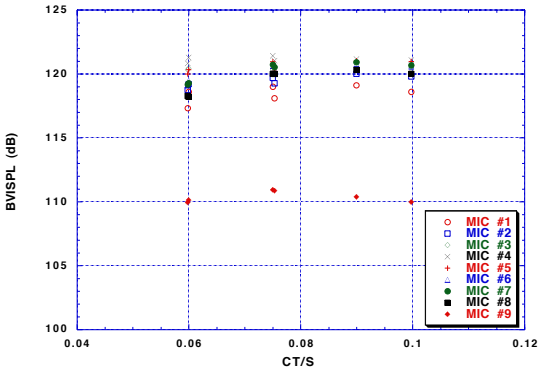

Fig 6a. BVISPL as function of C_T/σ at μ = 0.2 and α_{tpp} = 4°. 3-blade rotor. M_{tip} = 0.691. Traverse at r/R = 1.0.

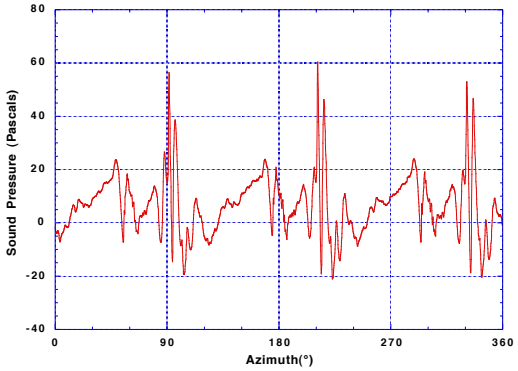

Fig 7. Unfiltered acoustic time history at the peak BVI condition (M_{tip} = 0.691, C_T/σ = 0.075, μ = 0.2, α_{tpp} = 4°). 3-blade rotor. Mic #9.

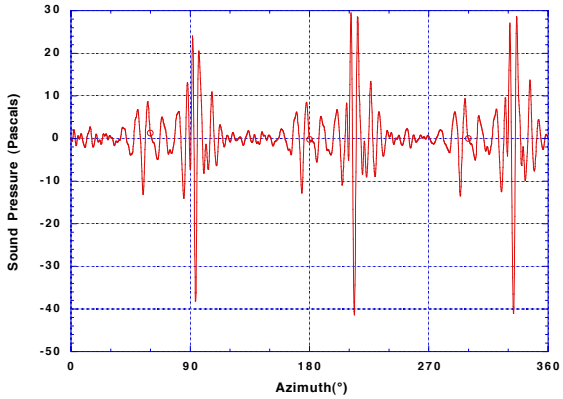

Fig 8(a). Filtered acoustic time history at the peak BVI condition (M_{tip} = 0.691, C_T/σ = 0.075, μ = 0.2, α_{tpp} = 4°). 3-blade rotor. Mic #9.

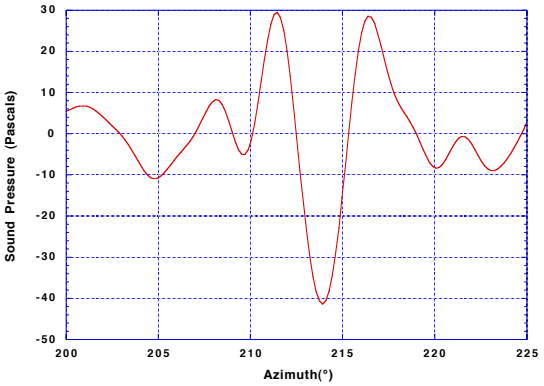

Fig 8(b). Expanded azimuth, middle pulse.

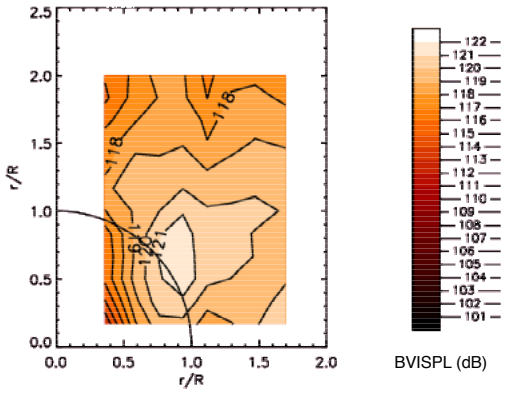

Fig 9. Acoustic footprint under advancing side of rotor. High BVI condition (M_{tip} = 0.691, C_T/σ = 0.075, μ = 0.2, α_{tpp} = 4°). 3-blade rotor.

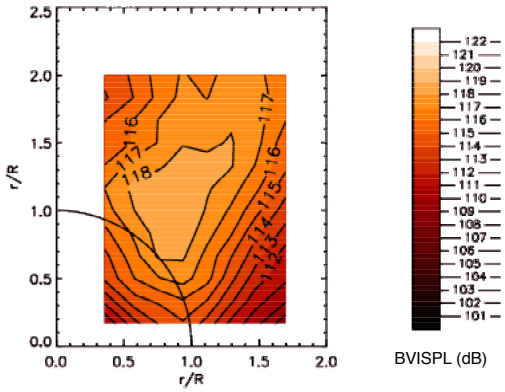

Fig 10. Acoustic footprint under advancing side of rotor. Moderate BVI condition (M_{tip} = 0.691, C_T/σ = 0.075, μ = 0.15, α_{tpp} = 3°). 3-blade rotor.

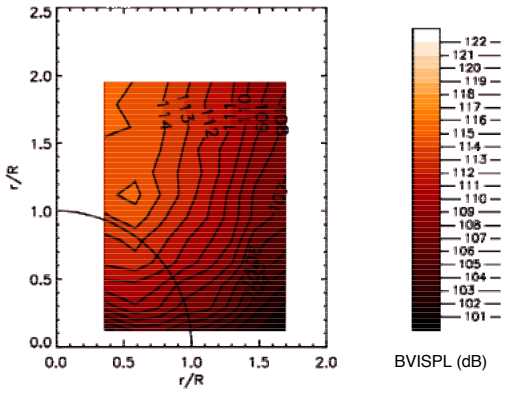

Fig 11. Acoustic footprint under advancing side of rotor. Low BVI condition (M_{tip} = 0.691, C_T/σ = 0.075, μ = 0.15, α_{tpp} = -3°). 3-blade rotor.

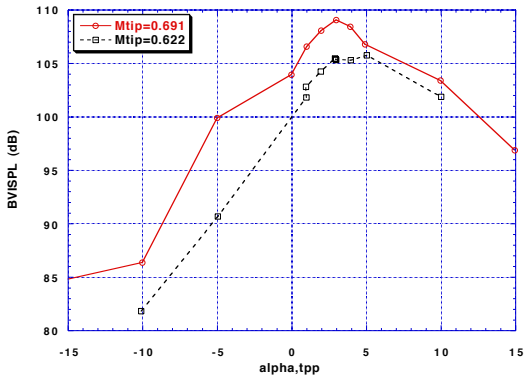

Fig 13. Effect or reduced M_{tip} on BVISPL. Fixed thrust = 4500 lbs and speed = 69 knots. 3-blade rotor. Mic #9.

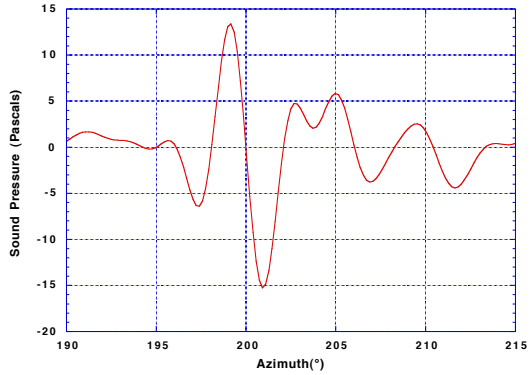

Fig 12. Filtered acoustic time history at the low BVI condition (M_{tip} = 0.691, C_T/σ = 0.075, μ = 0.15, α_{tpp} = -3°). 3-blade rotor. Mic #9. Expanded azimuth, middle pulse.

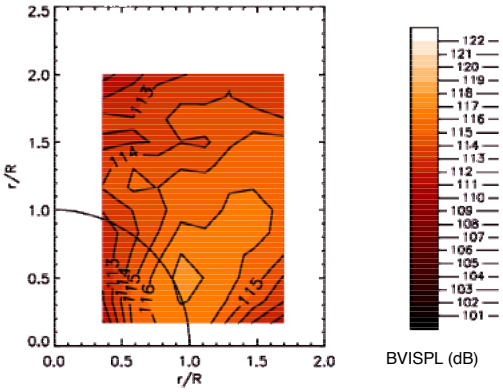

Fig 14. Acoustic footprint under advancing side of rotor. Reduced M_{tip}. 3-blade rotor. M_{tip} = 0.622, thrust = 4500 lbs, speed = 69 knots, α_{tpp} = 3°.

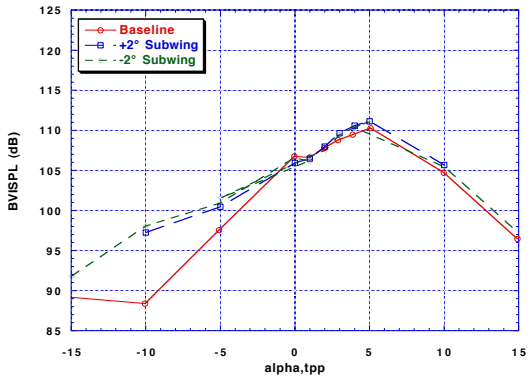

Fig 15. Comparison of two subwings with baseline rotor. M_{tip} = 0.691, C_T/σ = 0.09, μ = 0.17. Mic #9.

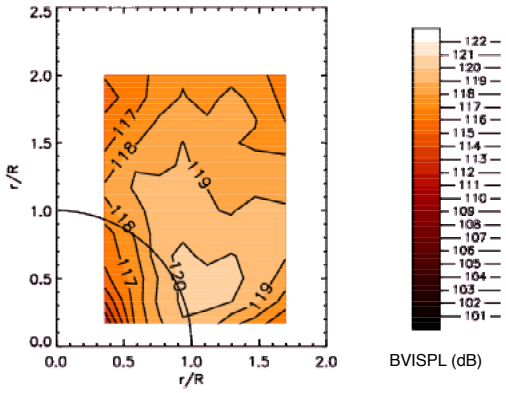

Fig 16. Acoustic footprint of baseline rotor. M_{tip} = 0.691, C_T/σ = 0.09 (thrust = 5500 lbs), μ = 0.17, α_{tpp} = 3°.

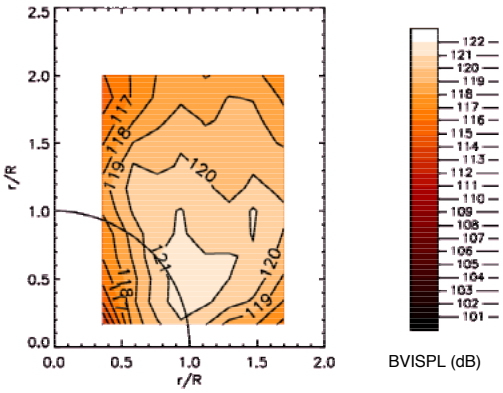

Fig 17. Acoustic footprint of rotor with +2° subwings. M_{tip} = 0.691, C_T/σ = 0.09, μ = 0.17, α_{tpp} = 3°.

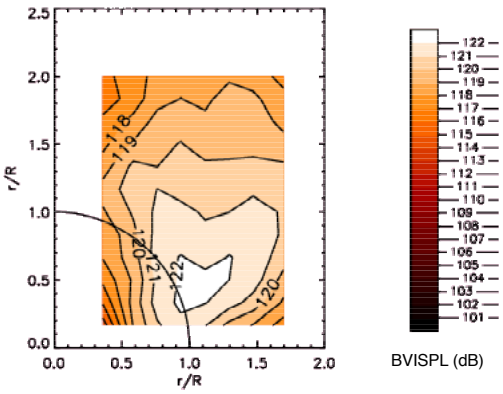

Fig 18. Acoustic footprint of rotor with -2° subwings. M_{tip} = 0.691, C_T/σ = 0.09, μ = 0.17, α_{tpp} = 3°.

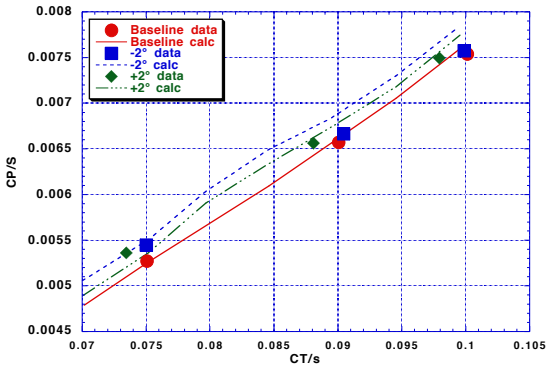

Fig 19. Effect of subwings on rotor performance. M_{tip} = 0.691, μ = 0.17, α_{tpp} = -10°.

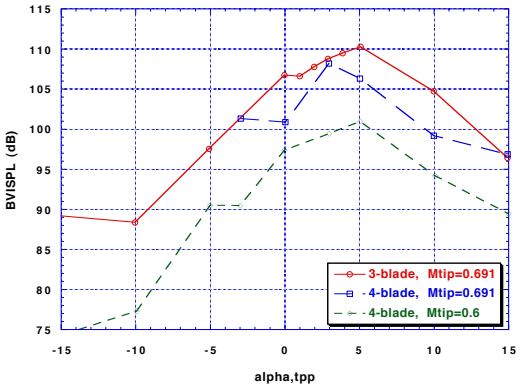

Fig 20. Comparison of 4-blade rotor with 3-blade rotor at fixed thrust = 5500 lbs and speed = 77 knots. Mic #9.

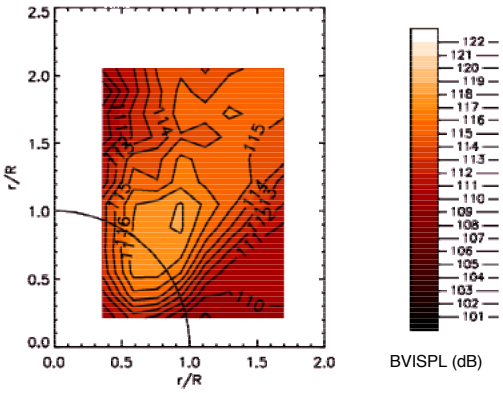

Fig 21. Acoustic footprint of 4-blade rotor. M_{tip} = 0.691, thrust = 5500 lbs, speed = 77 knots, α_{tpp} = 3°.

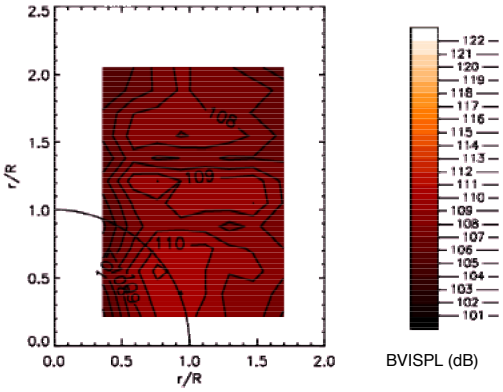

Fig 22. Acoustic footprint of 4-blade rotor. M_{tip} = 0.6, thrust = 5500 lbs, speed = 77 knots, α_{tpp} = 3°.